Fast reconstruction of multiple off-axis holograms based on a combination of complex encoding and digital spatial multiplexing

Bei Sha (沙 贝)[1,2], Yujie Lu (鲁玉洁)[1], Yiyan Xie (谢一言)[1], Qingyang Yue (岳庆炀)[1], and Chengshan Guo (国承山)[1,*]

[1]*College of Physics and Electronics, Shandong Normal University, Jinan 250014, China*
[2]*College of Physics and Electronic Engineering, Qilu Normal University, Jinan 250200, China*
**Corresponding author: guochsh@sdnu.edu.cn*

Received February 25, 2016; accepted April 8, 2016; posted online May 18, 2016

An algorithm is proposed for the fast reconstruction of off-axis digital holograms based on a combination of complex encoding (CE) and spatial multiplexing (SM). In this algorithm, every two off-axis holograms recorded in sequence are first assembled into a CE hologram using the CE method, and then four of the CE holograms are again encoded into one complex spatial multiplexing (CSM) hologram based on the SM algorithm. It is demonstrated that the eight holograms encoded into such one CSM hologram can be quickly reconstructed by performing a two-dimensional (2D) Fourier transform (FT) on the CSM hologram. Using this method, the eight 2D FTs required for the reconstruction of the eight holograms in the conventional spatial filtering methods can be simplified to a process with only one 2D FT, which can largely improve the computation efficiency with the resolution of the reconstructed images nearly unchanged.

OCIS codes: 090.1995, 090.4220, 200.3050.
doi: 10.3788/COL201614.060902.

Digital holography (DH) has drawn much attention in recent years due to its unique capability for digitally retrieving the complex amplitude distribution transmitted or scattered by a sample. Its applications have been extended to many areas, such as contour measurement[1–5], digital microscopy[6–9], image recognition[10–12], x ray imaging[13–15], electron microscopy[16–18], and various noninvasive measurements[19–21]. According to the relative orientations between the object beam and the reference beam in a holographic recording system, DHs are often divided into two categories: on-axis and off-axis. The former is capable of effectively utilizing the spatial frequency bandwidth of image sensors and thus can capture finer sample spatial details, but it suffers from the disturbance of the zero-order autocorrelation and the conjugate image, which need to be eliminated by using phase-shifting techniques or other time-consuming elimination algorithms[22–26]. In off-axis DHs, the autocorrelation and the conjugate items are separated from the required image item in the spatial frequency domain and thus can be eliminated simply by digital spatial filtering[27–30], although the off-axis geometry will result in an extra demand for the bandwidth of imaging sensors.

In the reconstruction of the recorded wavefront from an off-axis hologram based on spatial filtering, at least a two-dimensional (2D) Fourier transform (FT) is required, which is usually a time-consuming operation, especially for a hologram with a large number of pixels. Although such a reconstruction process could be speeded up to video rate using parallel computing techniques, some special graphic processing units and high programming skill are required. Recently, Girshovitz *et al.* proposed a novel and effective method for speeding up the reconstruction of off-axis digital holograms based on digital angular multiplexing (AM)[31] and a complex encoding (CE)[32] algorithm, which realizes the quick reconstruction of up to four holograms at the same time. This approach greatly increases the reconstruction efficiency and makes it possible to realize a real-time holographic reconstruction with a personal computer. In this paper, we present a complex spatial multiplexing (CSM) method for the fast reconstruction of off-axis holograms based on a combination of the CE algorithm and the spatial multiplexing (SM) algorithm[33]. Using this method, up to eight holograms can be encoded into one complex hologram and synchronously reconstructed, and so the reconstruction efficiency can be further improved.

Suppose that the interference intensity of an off-axis digital hologram recorded by an image sensor is

$$H_t(x,y) = R^2 + |O_t(x,y)|^2 + O_t(x,y)R\exp(-i2\pi\xi_0 x) + O_t^*(x,y)R\exp(i2\pi\xi_0 x), \quad (1)$$

where $O_t(x,y)$ is the complex amplitude of the sample recorded at time t, and R is the amplitude of the reference beam. For the sake of simplicity, we assume that the reference beam is a plane wave tilted in the x direction with a carrier frequency of ξ_0. If the bandwidth of the recorded object wave is equal to $2\xi_m$, the size of ξ_0 is usually set to one and a half times the bandwidth for an ideal off-axis hologram, that is, $\xi_0 = 3\xi_m$. For extracting the sample's complex amplitude from such an off-axis hologram, it is necessary to first transform Eq. (1) into its spatial

frequency domain by a 2D FT. The spatial frequency of the hologram H_t can be expressed as

$$\begin{aligned}\tilde{H}_t = \mathbb{F}\{H_t\} &= \mathbb{F}\{R^2 + |O_t|^2\} + R\mathbb{F}\{O_t\} \otimes \delta(\xi + \xi_0) \\ &\quad + R\mathbb{F}\{O_t^*\} \otimes \delta(\xi - \xi_0) \\ &= C_t(\xi,\eta) + R\tilde{O}_t(\xi,\eta) \otimes \delta(\xi + 3\xi_m) \\ &\quad + R\tilde{O}_t^*(\xi,\eta) \otimes \delta(\xi - 3\xi_m), \end{aligned} \tag{2}$$

where $\mathbb{F}\{\xi,\eta\}$ denotes the FT operation, $\otimes$ is the convolution operator, $C_t(\xi,\eta)$ is the autocorrelation item determined by the first two items in Eq. (1), $\tilde{O}_t(\xi,\eta)$ and $\tilde{O}_t^*(\xi,\eta)$ are the FTs of $O_t(x,y)$ and $O_t^*(x,y)$. The delta functions of $\delta(\xi+\xi_0)$ and $\delta(\xi-\xi_0)$ mean the frequency shifts of $\tilde{O}_t(\xi,\eta)$ and $\tilde{O}_t^*(\xi,\eta)$, respectively, introduced by the carrier frequency ξ_0 of the reference beam. Figure 1(a) shows a sketch of the spatial spectrum of the hologram H_t, in which ξ_0 is set to three times the maximum frequency of the recorded sample ξ_m. It can be seen that, in this situation, the spatial spectrum of the sample could be directly extracted from the spatial spectrum of the hologram by spatial filtering[27–30], and then the recorded complex amplitude of the sample wave can be reconstructed by a further inverse FT. That is to say, two 2D FTs are needed for the retrieval of the complex amplitude of the sample wave from each hologram based on the conventional spatial filtering methods. However, 2D FTs are often time-consuming operations, especially for a hologram with a large number of pixels.

To improve the reconstruction efficiency of the off-axis holograms, we propose the CSM algorithm based on a combination of the CE algorithm and the SM algorithm. In this CSM algorithm, we first assemble eight off-axis holograms $H_i(x,y)$ $(i=1,2,\ldots,8)$, recorded in sequence into four CE functions as follows:

$$\begin{cases} H_{1,2} = H_1 + jH_2 \\ H_{3,4} = H_3 + jH_4 \\ H_{5,6} = H_5 + jH_6 \\ H_{7,8} = H_7 + jH_8 \end{cases}, \tag{3}$$

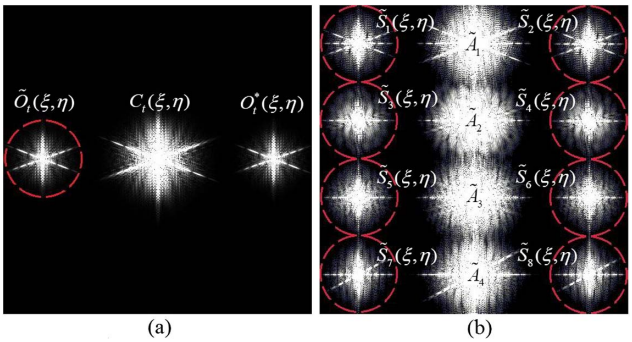

Fig. 1. Sketch of the spatial spectrum of (a) a conventional ideal off-axis hologram and (b) a CSM hologram encoded by eight off-axis holograms.

where the sign j represents the unit's imaginary number; then, these four CE functions are further synthesized into a CSM function. This function is constructed by adding four complex holograms, each of which is multiplied by a plane wave tilted in the y direction (orthogonal to the tilt direction of the reference beam in a holographic recording). The CSM function can be expressed as

$$\begin{aligned} H = {} & H_{1,2}\exp(-j6\pi\xi_m y) + H_{3,4}\exp(-j2\pi\xi_m y) \\ & + H_{5,6}\exp(j2\pi\xi_m y) + H_{7,8}\exp(j6\pi\xi_m y). \end{aligned} \tag{4}$$

Thus, all the information of the eight holograms is encoded in one CSM function. Next, we will prove that the object waves recorded in the eight holograms can be retrieved from the spatial spectrum of the CSM function, which means only one 2D FT is required for the reconstruction of the eight holograms.

By substituting Eqs. (1) and (3) into Eq. (4), the CSM function can be further written as

$$\begin{aligned} H = {} & A_1\exp[-j6\pi\xi_m y] + S_1\exp[-j2\pi(\xi_0 x + 3\xi_m y)] \\ & + S_2\exp[j2\pi(\xi_0 x - 3\xi_m y)] + A_2\exp[-j2\pi\xi_m y] \\ & + S_3\exp[-j2\pi(\xi_0 x + \xi_m y)] \\ & + S_4\exp[j2\pi(\xi_0 x - \xi_m y)] + A_3\exp[j2\pi\xi_m y] \\ & + S_5\exp[-j2\pi(\xi_0 x - \xi_m y)] \\ & + S_6\exp[j2\pi(\xi_0 x + \xi_m y)] + A_4\exp[j6\pi\xi_m y] \\ & + S_7\exp[-j2\pi(\xi_0 x - 3\xi_m y)] \\ & + S_8\exp[j2\pi(\xi_0 x + 3\xi_m y)], \end{aligned} \tag{5}$$

where A_i $(i=1,2,3,4)$ correspond to the autocorrelation items of the original holograms. S_i $(i=1,2,\ldots,8)$ are determined by the following formula:

$$\begin{cases} S_1 = O_1 + jO_2, & S_2 = O_1^* + jO_2^* \\ S_3 = O_3 + jO_4, & S_4 = O_3^* + jO_4^* \\ S_5 = O_5 + jO_6, & S_6 = O_5^* + jO_6^* \\ S_7 = O_7 + jO_8, & S_8 = O_7^* + jO_8^* \end{cases}. \tag{6}$$

Obviously, for retrieving the object waves of the encoded holograms, all the components S_i $(i=1,2,\ldots,8)$ expressed in Eq. (6) should be firstly separated from the CSM function, which could be realized by spatial filtering in the spatial frequency domain.

The spatial frequency of the CSM function is just equal to the FT of Eq. (5), which can be expressed as

$$\begin{aligned} \tilde{H} = {} & \mathbb{F}\{H\} \\ = {} & [\tilde{A}_1 + R\tilde{S}_1 \otimes \delta(\xi+\xi_0) + R\tilde{S}_2 \otimes \delta(\xi-\xi_0)] \otimes \delta(\eta+3\xi_m) \\ & + [\tilde{A}_2 + R\tilde{S}_3 \otimes \delta(\xi+\xi_0) + R\tilde{S}_4 \otimes \delta(\xi-\xi_0)] \otimes \delta(\eta+\xi_m) \\ & + [\tilde{A}_3 + R\tilde{S}_5 \otimes \delta(\xi+\xi_0) + R\tilde{S}_6 \otimes \delta(\xi-\xi_0)] \otimes \delta(\eta-\xi_m) \\ & + [\tilde{A}_4 + R\tilde{S}_7 \otimes \delta(\xi+\xi_0) + R\tilde{S}_8 \otimes \delta(\xi-\xi_0)] \otimes \delta(\eta-3\xi_m), \end{aligned} \tag{7}$$

where $\tilde{S}_i = \mathbb{F}\{S_i\}$ $(I = 1, 2..., 8)$. Figure 1(b) gives a sketch of the spatial spectrum of the CSM function. It can be seen that the spatial spectra $\tilde{S}_i$ of all the components S_i are spatially separated in the spatial frequency domain, and so they can be extracted by spatial filtering. The spatial spectra $\tilde{O}_i$ of the object waves recorded by the eight holograms can be retrieved according to the following formula:

$$\begin{cases} \tilde{O}_1(\xi,\eta) = \frac{1}{2}[\tilde{S}_1(\xi,\eta) + \tilde{S}_2(-\xi,-\eta)^*] \\ \tilde{O}_2(\xi,\eta) = \frac{1}{2j}[\tilde{S}_1(\xi,\eta) - \tilde{S}_2(-\xi,-\eta)^*] \\ \tilde{O}_3(\xi,\eta) = \frac{1}{2}[\tilde{S}_3(\xi,\eta) + \tilde{S}_4(-\xi,-\eta)^*] \\ \tilde{O}_4(\xi,\eta) = \frac{1}{2j}[\tilde{S}_3(\xi,\eta) - \tilde{S}_4(-\xi,-\eta)^*] \\ \tilde{O}_5(\xi,\eta) = \frac{1}{2}[\tilde{S}_5(\xi,\eta) + \tilde{S}_6(-\xi,-\eta)^*] \\ \tilde{O}_6(\xi,\eta) = \frac{1}{2j}[\tilde{S}_5(\xi,\eta) - \tilde{S}_6(-\xi,-\eta)^*] \\ \tilde{O}_7(\xi,\eta) = \frac{1}{2}[\tilde{S}_7(\xi,\eta) + \tilde{S}_8(-\xi,-\eta)^*] \\ \tilde{O}_8(\xi,\eta) = \frac{1}{2j}[\tilde{S}_7(\xi,\eta) - \tilde{S}_8(-\xi,-\eta)^*] \end{cases}, \quad (8)$$

where $\tilde{S}_i(-\xi,-\eta)^* = [\tilde{S}_i(-\xi,-\eta)]^*$. Finally, the complex amplitude O_i of the object waves can be reconstructed by an inverse FT of the corresponding spatial spectrum $\tilde{O}_i$.

Figure 2 gives the flowchart of the CSM algorithm described above, which mainly contains the following steps: (A) encode eight holograms H_i $(i = 1, 2, ..., 8)$ into one CSM function H using the CSM encoding algorithm shown in Eqs. (3) and (4); (B) get the spatial spectrum of the CSM function by calculating a 2D fast FT; (C) extract the components $\tilde{S}_i$ from the spatial spectrum of the CSM function as shown in Fig. 1(b); (D) retrieve the spatial spectra $\tilde{O}_i$ of the object waves from the data $\tilde{S}_i$ based on Eq. (8); (E) if required, take further steps such as inversely transforming $\tilde{O}_i$ to get the complex amplitudes of the object wave O_i, unwrapping the phase distributions, and enlarging them for display.

Experiments were carried out to demonstrate the method described above. The holographic recording setup used in the experiments is shown in Fig. 3, which is essentially a Mach–Zehnder interferometer. In our experiments, the light source is an He–Ne laser with a wavelength of 632.8 nm. The recorded object is a dynamic refractive index field produced by a flame, which is imaged on the recording plane by an imaging lens and interferes with a tilted plane wave. The holograms were recorded by a CCD image sensor with a pixel size of 6.45 μm × 6.45 μm and pixel number of 1024 × 1024.

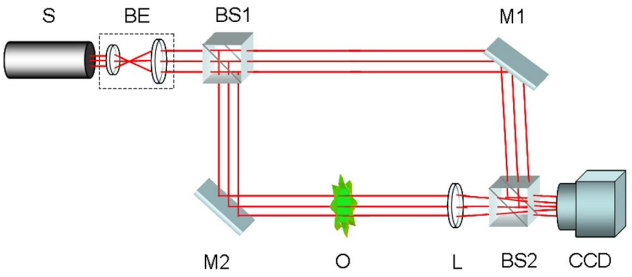

Fig. 3. Off-axis holographic recording setup used in experiments for CSM algorithm. S, source; BE, beam expander; BS, beam splitter; M, mirror; L, lens; CCD, image sensor.

A series of off-axis holograms was recorded in sequence, one of which is shown in Fig. 4(a). For the reconstruction of the holograms using our CSM algorithm described above, we first divided them into groups: each group contains eight holograms. Then we encode the eight holograms in each group into a CSM function according to Eqs. (3) and (4) and calculate the spatial spectrum of the CSM function. Figure 4(b) shows an example of the spatial spectrum of a CSM function of the recorded holograms in experiments. Using the eight parts marked by the red circles in Fig. 4(b), the frequency spectra of the complex amplitude distributions of the object waves recorded in the eight holograms can be synchronously retrieved according to Eq. (8). Next, we can obtain the complex amplitude distributions by carrying the inverse FT operation on each of the eight retrieved frequency spectra. Figures 5(a)–5(h) give the phase distributions of the object waves reconstructed from a group of holograms using our CSM algorithm.

To test the phase reconstruction quality of the CSM algorithm, we compared the phase profile retrieved by using the CSM algorithm with that retrieved using the

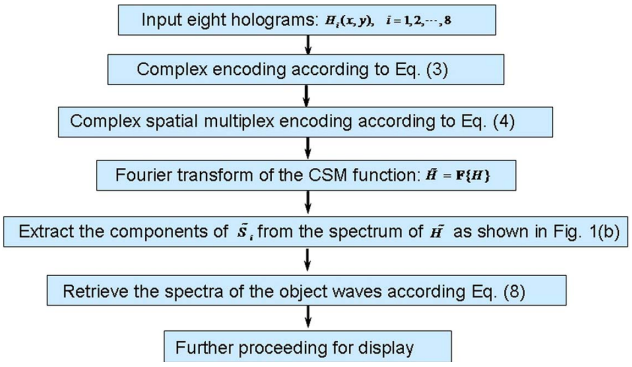

Fig. 2. Flowchart of the CSM algorithm for fast reconstruction of off-axis holograms.

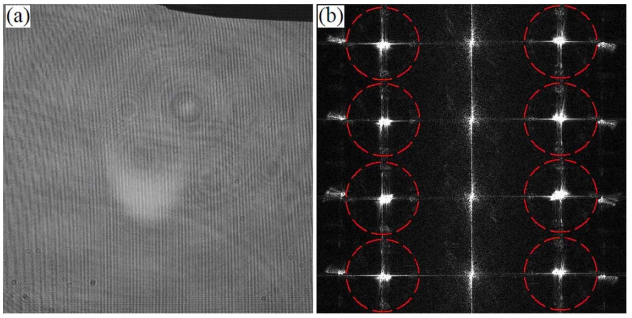

Fig. 4. (a) Example of the off-axis holograms recorded in the experiment. (b) Example of the spatial spectrum of a CSM function encoded by eight recorded holograms.

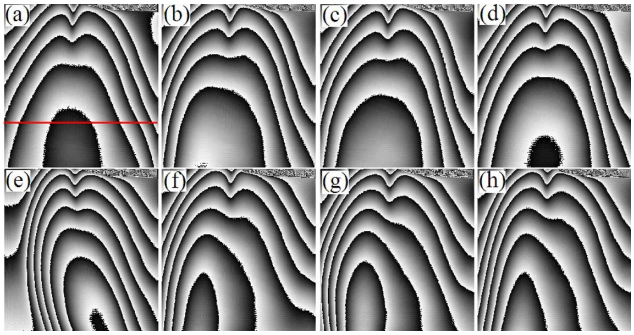

Fig. 5. One group of the reconstructed wrapped phases using the CSM algorithm.

conventional spatial filtering algorithm (below we abbreviate it to CV algorithm) from the same hologram. In the CSM algorithm, eight different holograms are synchronously reconstructed by one 2D FT, while in the CV algorithm, the holograms are separately reconstructed one by one. One of the compared results is shown in Fig. 6, which shows a phase profile of the retrieved object wave as shown in Fig. 5(a) (the part along the red line). In Fig. 6, the blue line expresses the phase value retrieved based on the CSM algorithm and the red dashed line corresponds to the result using the CV method. It can be seen that the phase reconstructed by the CSM algorithm is consistent with that reconstructed by the conventional algorithm. Meanwhile, the computation efficiency of the CSM algorithm is greatly improved.

To test the influence of the CSM algorithm on the resolution of the reconstructed images when eight holograms are synchronously reconstructed, we changed the phase object to a transmittance USAF resolution target (with group numbers of 2 to 7) and repeated the experiment. In this experiment, the lens L shown in Fig. 3 was also removed, and the distance between the target and the recording plane was set to about 175 mm. Figure 7(a) gives an example of the images reconstructed based on the CSM algorithm. As a comparison, Fig. 7(b) shows the image reconstructed from the same hologram but based on the

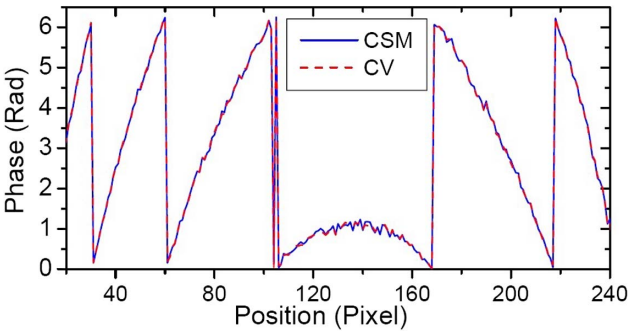

Fig. 6. Example of the compared results of the retrieved phases using the CSM algorithm (the blue line) with that using the CV method (the red dashed line) at the same position of the retrieved phase distributions from the same hologram as the part marked by the red line in Fig. 5(a).

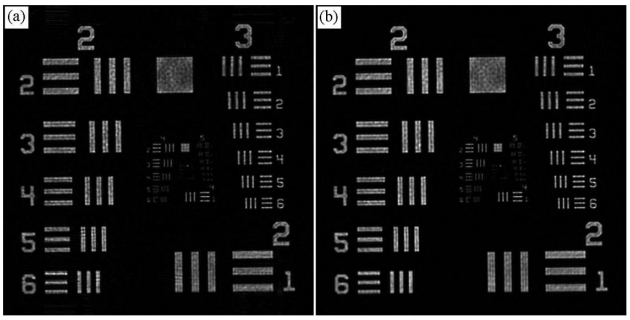

Fig. 7. Examples of the images reconstructed by using (a) the CSM algorithm and (b) the CV algorithm when the object is a transmittance USAF resolution target with group numbers of 2 to 7.

CV algorithm. It can be seen that the image reconstructed by the CSM algorithm has the same resolution as that reconstructed using the CV algorithm.

Last, we compared the computation efficiency of the CSM algorithm with that of the CV algorithm, the AM algorithm[31], the complex angular multiplexing (CAM) algorithm[32], and the SM algorithm[33] under the same hardware and software environments. The compared processing times were firstly taken from encoding the holograms to getting the complex amplitudes of the object waves recorded in the holograms and then divided by the number of holograms. In order to compare the influence of the hologram size on the computation efficiency, holograms of different sizes were simulated in computer. Table 1 shows the average ratio of the CSM's processing time (t_{CSM}) to the CV's processing time (t_{CV}), the AM's processing time (t_{AM}), the CAM's processing time (t_{CAM}), and the SM's processing time (t_{SM}). The sizes of the holograms are set to 512×512, 1024×1024, and 2048×2048. All the calculations involved in Table 1 was performed in a single-core personal computer (Pentium4 2.8 GHz CPU, 2 GB RAM).

It can be seen from Table 1 that the computation efficiency of our CSM algorithm is superior to that of the other four algorithms. For example, the CSM algorithm on average takes only about twelve percent of the processing time cost by the CV algorithm for reconstructing one hologram and less than fifty percent of the CAM's processing time.

Table 1. Ratio of the CSM's Processing Time to Other Algorithms' for Reconstructing a Single Off-Axis Hologram

Size	t_{CSM}:t_{CV} (%)	t_{CSM}:t_{AM} (%)	t_{CSM}:t_{CAM} (%)	t_{CSM}:t_{SM} (%)
512×512	10.7	39.1	44.9	77.0
1024×1024	11.9	42.5	48.5	77.4
2048×2048	12.1	40.8	45.7	75.8

In conclusion, we demonstrate that the off-axis holograms can be quickly reconstructed by the CSM algorithm, in which only one 2D FT is required for getting the spatial spectra of eight holograms by encoding them into a CSM function based on a combination of the CE algorithm and SM algorithm; thus, a great deal of unnecessary calculations can be cut out and the computational efficiency is greatly improved. We think that this improved algorithm may be useful in the implementation of real-time holographic visualizations in a simple personal computer system. In particular, it can be a good choice in the design of a preview system for dynamic wavefront imaging in digital holographic microscopy. In addition, the CSM algorithm can also provide an approach for compressing off-axis holograms in optical information storage and processing.

The work was supported by National Natural Science Foundation of China under Grant No. 11474186.

References

1. S. M. Solís, M. S. Hernández-Montes, and F. M. Santoyo, Biomed. Opt. Express **3**, 3203 (2012).
2. D. G. Abdelsalam, J. Min, D. Kim, and B. Yao, Chin Opt. Lett. **13**, 100701 (2015).
3. G. Nehmetallah, P. P. Banerjee, D. Ferree, R. Kephart, and S. Praharaj, Chin Opt. Lett. **9**, 120004 (2011).
4. D. G. Abdelsalam, J. Min, D. Kim, and B. Yao, Chin Opt. Lett. **13**, 100701 (2015).
5. Z. Wang, Y. Chen, and Z. Jiang, Chin Opt. Lett. **14**, 010008 (2016).
6. C. A. Trujillo and J. Garcia-Sucerquia, Opt. Lett. **39**, 2569 (2014).
7. E. Sánchez-Ortiga, A. Doblas, G. Saavedra, M. Martínez-Corral, and J. Garcia-Sucerquia, Appl. Opt. **53**, 2058 (2014).
8. D. C. Clark and M. K. Kim, Chin Opt. Lett. **9**, 120001 (2011).
9. J. Ma, C. Yuan, G. Situ, G. Pedrini, and W. Osten, Chin Opt. Lett. **11**, 090901 (2013).
10. A. Anand and B. Javidi, Chin. Opt. Lett. **12**, 060012 (2014).
11. C. Su, X. Xia, H. Li, X. Liu, C. Kuang, J. Xia, and B. Wang, Chin. Opt. Lett. **12**, 060007 (2014).
12. M. Seifi, L. Denis, and C. Fournier, J. Opt. Soc. Am. A **30**, 2216 (2013).
13. W. F. Schlotter, J. Lüning, R. Rick, K. Chen, A. Scherz, S. Eisebitt, C. M. Günther, W. Eberhardt, O. Hellwig, and J. Stöhr, Opt. Lett. **32**, 3110 (2007).
14. E. Guehrs, C. M. Gunther, R. Konnecke, B. Pfau, and S. Eisebitt, Opt. Express **17**, 6710 (2009).
15. D. Pelliccia, L. Rigon, F. Arfelli, R. H. Menk, I. Bukreeva, and A. Cedola, Opt. Express **21**, 19401 (2013).
16. Z. Gan, D. E. Perea, J. Yoo, S. T. Picraux, D. J. Smith, and M. R. McCartney, Appl. Phys. Lett. **103**, 153108 (2013).
17. A. Pantzer, A. Vakahy, Z. Eliyahou, G. Levi, D. Horvitz, and A. Kohn, Ultramicroscopy **138**, 36 (2014).
18. F. Röder, A. Lubk, D. Wolf, and T. Niermann, Ultramicroscopy **144**, 32 (2014).
19. Y. Wang, D. Wang, J. Zhao, Y. Yang, X. Xiao, and H. Cui, Chin Opt. Lett. **9**, 030901 (2011).
20. Z. Lu, J. Sun, Y. Zhou, N. Zhang, Z. Sun, and L. Liu, Chin Opt. Lett. **13**, 020901 (2015).
21. L. Yao, X. Wu, J. Yang, Y. Wu, X. Gao, L. Chen, G. Gréhan, and K. Cen, Chin Opt. Lett. **13**, 072801 (2015).
22. X. F. Xu, L. Cai, Y. Wang, X. Meng, W. J. Sun, H. Zhang, X. Cheng, G. Dong, and X. Shen, Opt. Lett. **33**, 776 (2008).
23. J. Deng, H. Wang, D. Zhang, L. Zhong, J. Fan, and X. Lu, Opt. Lett. **38**, 1506 (2013).
24. C. S. Guo, B. Sha, Y. Y. Xie, and X. T. Zhang, Opt. Lett. **39**, 813 (2014).
25. E. Stoykova, H. Kang, and J. Park, Chin. Opt. Lett. **12**, 060013 (2014).
26. Y. Li, W. Xiao, F. Pan, and L. Rong, Chin Opt. Lett. **12**, 020901 (2014).
27. E. Cuche, P. Marquet, and C. Depeursinge, Appl. Opt. **39**, 4070 (2000).
28. N. Verrier and M. Atlan, Appl. Opt. **50**, H136 (2011).
29. H. Pham, H. Ding, N. Sobh, M. Do, S. Patel, and G. Popescu, Biomed. Opt. Express **2**, 1781 (2011).
30. I. Frenklach, P. Girshovitz, and N. T. Shaked, Opt. Lett. **39**, 1525 (2014).
31. P. Girshovitz and N. T. Shaked, Opt. Lett. **39**, 2262 (2014).
32. P. Girshovitz and N. T. Shaked, Opt. Express **23**, 8773 (2015).
33. B. Sha, X. Liu, X. L. Ge, and C. S. Guo, Opt. Express **22**, 23066 (2014).